Transient simulation for large scale flow in bubble columns

T. Ziegenhein, R.Rzehak, D.Lucas

Helmholtz-Zentrum Dresden-Rossendorf e.V. 01314 Dresden Germany

Abstract

The transient simulation of large scale bubbly flow in bubble columns using the unsteady Reynolds averaged Navier Stockes (URANS) equations is investigated in the present paper. An extensive set of bubble forces is used with different models for the bubble induced turbulence. Criteria are given to assess the independence of the simulation time and the time step length. Using these criteria it is shown that a simulation time, time step length and mesh independent solution can be obtained for complex bubbly flows using URANS equations under certain requirements. With the obtained setup the contribution of the resolved turbulence to the total turbulence and the influence of the bubble induced turbulence modeling on the resolved turbulence is investigated. Further, it is pointed out that the virtual mass force is not negligible. The simulations are compared to data from the literature at two different superficial velocities, which cover monodisperse and polydisperse bubbly flows.

Keywords: bubble columns, bubble induced turbulence, transient multiphase flow, Euler-Euler modeling, CFD simulation, model validation

Email address: `t.ziegenhein@hzdr.de` (T. Ziegenhein, R.Rzehak, D.Lucas)

1. Introduction

Problems involving multiphase flows occur in a great variety of technical and natural processes. A common flow regime is that a disperse phase exists in a continuous phase. Modeling such multiphase flows is an active area of research. In the present paper the focus is on the modeling and description of turbulent structures on the scale of an apparatus like a bubble column and the influence of the modeling of the small scales on the large scale dynamics.

A widely used approach for modeling dispersed multiphase flows on large scale is the Eulerian two-fluid approach. Here the conservation equations are formulated for each phase and are weighted with the volume fraction of the corresponding phase. The interaction between the phases appears as sink and source terms in the conservation equations. To simulate large scale applications the small scales are averaged and the interface between gas and liquid is not resolved. Therefore, the small scale interactions between the gas and liquid phase have to be completely treated in closure models.

Turbulence for large scale simulations is usually described with the Reynolds averaged Navier Stockes (RANS) equations. Although the model is fully time-dependent, typically only steady state problems are considered. The reason is that the model constants have been calibrated by comparison to stationary situations (Launder and Spalding (1974)). When applied to unsteady problems the URANS frequently gives reasonable results for the time dependence at much lower computational cost then LES (Spalart (2000)). In the context of bubble columns simulations with the Eulerian two-fluid approach and the URANS turbulence description with a two equation turbulence model have been initiated by Sokolichin and Eigenberger (1999) and are used until today for example by Masood and Delgado (2014). In the present work the SST two equation turbulence model is used with additional source terms modeling the bubble induced turbulence.

Especially in gravity driven bubbly flows a distinct transient behavior can be identified through large scale circulation, as reviewed by Mudde (2005). Also, through the uneven aeration naturally caused by the sparger in larger bubble columns a distinct periodic plume occurs which is studied for example by Julia et al. (2007). Therefore, an influence of the transient processes can be assumed and the usual steady solution could not cover such effects.

A proper turbulence modeling in dispersed multiphase flows is essential for a correct prediction of the momentum exchange between the phases. Especially for bubbly flows the break-up and coalescence processes, which are responsible for the bubble size distribution, are dominated by turbulence (Liao and Lucas (2010), Liao et al. (2011)). Because all modeled forces depend on the bubble size, the importance of a reliable turbulence prediction is underlined. In bubble columns the large scale structures, as described for example by Joshi et al. (2002), are also very important for mixing in technical apparatuses. Mixing might be under-predicted if these large scale fluctuations are suppressed by a steady solution method.

The motivation of the present study is therefore to show that (i) a steady solution is not sufficient under certain circumstances, (ii) with the URANS solution method the transient behavior can be covered and (iii) a solution time, time step length and mesh size independent solution can be obtained for complex multiphase flows. In addition, the bubble induced turbulence modeling is investigated and a model with source terms in the turbulence equations is shown to be necessary. Further, it is shown that the virtual mass force is not negligible, in contrast to the conclusion of several recent publications (e.g. Tabib et al. (2008) or Masood and Delgado (2014)). The application is the simulation of large scale reactors with distinct transient behavior, where Large Eddy Simulation with the Euler-Lagrange treatment is too cost-intensive.

The paper is structured as follows. In Section 2 the physical modeling is presented, in Section 3 the numerical setup is presented, in Section 4 the results are shown and compared with the experiments and finally in Section 5 the results are discussed and conclusions are drawn.

2. Physical modeling

In the present work the Eulerian two-fluid model is used. This approach has been discussed in a number of books (e.g. Yeoh and Tu (2010)), while its application to bubble columns is covered in several reviews (e.g. of Joshi et al. (2001) or of Jakobsen et al. (2005)). A brief summary of the equations is given in the appendix Appendix A.1. As a result of the averaged description, closure models which describe the interaction between the dispersed phase and the liquid phase are needed. In general this concerns forces acting on the liquid and dispersed phases and the induced turbulence in the liquid as a result of the motion of the dispersed phase.

Modeling and validation of forces acting on a bubble were intensively studied over the last decade, for example by Tabib et al. (2008), Krepper et al. (2009) or Lucas and Tomiyama (2011). All forces act together to produce observable phenomena like for example the distribution of void fraction. Hence, an independent validation of each single force is not possible. Therefore, a set of models which has recently been applied with good success by Rzehak and Krepper (2013b) is used in this paper, with the addition of the virtual mass force.

For the bubble induced turbulence several approaches exist. In this paper the approach is used that the bubble induced turbulence is modeled with source terms in two-equation models. Recently Rzehak and Krepper (2013a) performed a detailed study of different bubble induced turbulence models and formulated an own model which turned out to be the most reliable model for their test cases.

All simulations are carried out in a fully three dimensional domain, which has been shown to be essential by Ekambara et al. (2005) by comparing two and three dimensional modeling. For computation a customized version of CFX 14.5 is used.

2.1. Two-phase turbulence

2.1.1. Using source terms

Concerning turbulence in bubbly flows it is sufficient to consider the continuous liquid phase, based on the small density and small spatial scales of the dispersed gas. Shear-induced turbulence is described by the SST model with parameters taking their usual single phase values. Bubble induced turbulence is included by additional source terms. The governing equations are given in Appendix A.2.

Concerning the source term describing bubble effects in the k-equation there is large agreement in the literature. A plausible approximation is provided by the assumption that all energy lost by the bubble due to drag is converted to turbulent kinetic energy in the wake of the bubble. Hence, the k-source becomes

$$S_L^k = F_L^{Drag} |\vec{u}_G - \vec{u}_L|. \tag{1}$$

For the ϵ-source a similar heuristic is used as for the single phase model, namely the k-source is divided by some time scale τ so that

$$S_L^\epsilon = \frac{C_{\epsilon B}(S_L^k)}{\tau}. \tag{2}$$

For use with the SST model, the ϵ-source is transformed to an equivalent ω-source which gives

$$S_L^\omega = \frac{1}{C_\mu k_L} S_L^\epsilon - \frac{\omega_L}{k_L} S_L^k. \tag{3}$$

This ω-source is used independently of the blending function in the SST model since it should be effective throughout the fluid domain.

Modeling of the time scale τ proceeds largely based on dimensional analysis. There are two velocity and two length scales for this problem, where one of each is related to the bubble and the other to the turbulent eddies, so four plausible time scales can be formed. All four time scales were compared by Rzehak and Krepper (2013b) and it was found that the best predictions were obtained for

$$\tau = \frac{d_B}{\sqrt{k_L}}. \tag{4}$$

This variant will be used also here together with a value $C_{\epsilon B} = 1.0$. The eddy viscosity is evaluated from the standard formula

$$\mu_L^{turb} = C_\mu \rho_L \frac{k_L^2}{\epsilon_L}. \tag{5}$$

2.1.2. Using additional viscosity

The addition of an extra contribution to the viscosity that describes the bubble induced turbulence is an often used alternative approach and is used for comparison in this study. The turbulent viscosity then is formulated as

$$\mu_L^{turb} = \mu_L^{turb,SinglePhase} + \mu_L^{turb,BIT}, \tag{6}$$

where the bubble induced turbulence is formulated using the model of Sato et al. (1981)

$$\mu_L^{turb,BIT} = 0.6\rho_L \alpha_G d_B \left| \vec{u_G} - \vec{u_L} \right|. \tag{7}$$

2.2. URANS

In general URANS calculations are based on the traditional RANS approach but treated as transient. Often the relativly simple and fast URANS calculations are even treated with stationary boundary conditions to study for example vortex shedding at bluff bodies which gives reasonable predictions as discussed by Spalart (2000).

With the URANS approach the fluctuations of the velocity are decomposed in resolved and unresolved parts. For comparison with experiments both fluctuation parts have to be considered to get the total fluctuation.

For transient simulations the time averaged kinetic energy is simply the sum of the squared averaged velocity and the average of the squared fluctuations. For the velocity w in one direction:

$$\frac{1}{2}\rho\overline{ww} = \frac{1}{2}\rho(\overline{w}\overline{w} + \overline{w'w'}). \tag{8}$$

Where $\overline{w}$ is the average over time and w' the fluctuation around the average. In the URANS approach a modeled and a resolved fluctuation are obtained.

The fluctuation can be written as the sum of these two components:

$$w' = \widetilde{w'} + w''. \tag{9}$$

Where $\widetilde{w'}$ denotes the resolved fluctuation and w'' the modeled fluctuation. Using this summation the turbulent kinetic energy for the velocity component w can be written as:

$$\overline{w'w'} = \overline{\widetilde{w'}\widetilde{w'} + \widetilde{w''w''}}. \tag{10}$$

Using a two equation turbulence model it is supposed that the modeled fluctuation is isotropic. With the modeled turbulent kinetic energy k_{mod} the unresolved, modeled turbulent kinetic energy in one direction is:

$$\widetilde{w''w''} = \frac{2}{3} k_{mod}. \tag{11}$$

The resolved part $\overline{\widetilde{w'}\widetilde{w'}}$ is obtained from the transient simulation. The root mean square of the fluctuation for the velocity component w is therefore:

$$\sqrt{\overline{w'w'}} = \sqrt{\overline{\widetilde{w'}\widetilde{w'} + \frac{2}{3}k_{mod}}} = \sqrt{\overline{\widetilde{w'}\widetilde{w'}} + \frac{2}{3}\overline{k_{mod}}}. \tag{12}$$

This relation will be used to compare the simulated velocity fluctuations with experimentally measured values.

2.3. Bubble forces

In the Eulerian two-fluid model the interaction of the bubbles and the liquid phase is modeled by exchange terms between the separate momentum conservation equations of the liquid and the gas phase. At this point the attempt of a complete description of all bubble forces published by Rzehak and Krepper (2013b) is adopted. That this extensive description is also suitable for bubble columns has already been shown in Ziegenhein et al. (2013b).

2.3.1. Drag force

The drag force is a momentum exchange because of a slip velocity between the gas and a liquid force. This is modeled with a momentum sink in the gas momentum equation:

$$F_{Drag} = -\frac{3}{4d_B} C_D \rho_L \alpha_G |\vec{u}_G - \vec{u}_L| (\vec{u}_G - \vec{u}_L). \tag{13}$$

The drag coefficient C_D for the bubble regime investigated here mainly depends on the Reynolds number and the Eötvös number. A correlation distinguishing different shape regimes has been suggested by Ishii and Zuber (1979), namely

$$C_D = max(C_{D,sphere}, C_{D,ellipse}), \tag{14}$$

where

$$C_{D,sphere} = \frac{24}{Re}(1 + 0.1Re^{0.75}) \tag{15}$$

$$C_{D,ellipse} = \frac{2}{3} Eo^{0.5}. \tag{16}$$

Tomiyama et al. (1998) validated this correlation and found good agreement except at high values of the Eötvös number.

2.3.2. Lift force

In a shear flow a bubble experiences a force lateral to the direction of flow. This effect is in general referred to as the lift force and described by the definition of Zun (1980):

$$F_{Lift} = -C_L \rho_L \alpha_G (\vec{u}_G - \vec{u}_L) \times rot(\vec{u}_L). \tag{17}$$

For a spherical bubble the shear lift coefficient C_L is positive so that the lift force acts in the direction of decreasing liquid velocity, i.e. in case of co-current pipe flow in the direction towards the pipe wall. Experimental (e.g.

Tomiyama (2002)) and numerical (e.g. Bothe et al. (2006)) investigations showed that the direction of the lift force changes its sign if a substantial deformation of the bubble occurs. From the observation of the trajectories of single air bubbles rising in simple shear flow of a glycerol water solution the following correlation for the lift coefficient was derived:

$$C_L = \begin{cases} min[0.288\,tanh(0.121Re, f(Eo_\perp)], & Eo_\perp < 4 \\ f(Eo_\perp), & 4 < Eo_\perp < 10 \\ -0.27, & Eo_\perp > 10 \end{cases}, \tag{18}$$

with

$$f(Eo_\perp) = 0.00105Eo_\perp^3 - 0.0159Eo_\perp^2 - 0.0204Eo_\perp + 0.474. \tag{19}$$

Here the modified Eötvös number given by

$$Eo_\perp = \frac{g(\rho_L - \rho_G)d_\perp^2}{\sigma}, \tag{20}$$

where $d_\perp$ is the maximum horizontal dimension of the bubble. It is calculated using an empirical correlation for the aspect ratio by Wellek et al. (1966)

$$d_\perp = d_B\sqrt[3]{1 + 0.163Eo^{0.757}}, \tag{21}$$

where Eo is the usual Eötvös number. The usual Eötvös number Eo is calculated with the bubble diameter d_B as the characteristic length, where the modified Eötvös number $Eo_\perp$ is calculated with the maximum horizontal dimension of the bubble as the characteristic length.

The experimental conditions on which Eq. 18 is based, were limited to the range $-5.5 \leq log_{10}Mo \leq -2.8, 1.39 \leq Eo \leq 5.74$ and values of the Reynolds number based on bubble diameter and shear rate $0 \leq Re \leq 10$. The water-air system at normal conditions has a Morton number $Mo = 2.63e^{-11}$ which is quite different. Nevertheless, for this case the diameter where the lift force changes its direction could be shown by Lucas and Tomiyama (2011) to be in good agreement with the model. As can be seen from Eq. 18 and Eq. 19 this diameter is about 5.8 mm.

2.3.3. Turbulent dispersion force

The turbulent dispersion force describes the effect of the turbulent fluctuations of liquid velocity on the bubbles. In Burns et al. (2004) an explicit expression is derived by Favre averaging the drag force, namely

$$F_{Disp} = -\frac{3}{4} C_D \frac{\alpha_G}{d_B} |\vec{u}_G - \vec{u}_L| \frac{\mu_L^{turb}}{\sigma_{TD}} \left(\frac{1}{\alpha_L} + \frac{1}{\alpha_G} \right) \nabla \left(\alpha_G \right). \tag{22}$$

In analogy to molecular diffusion σ_{TD} is referred to as a Schmidt number. In principle it should be possible to obtain its value from single bubble experiments by evaluating the statistics of bubble trajectories in well characterized turbulent flows but to the authors knowledge this has not been done yet. A value of $\sigma_{TD} = 0.9$ is typically used.

2.3.4. Wall force

A bubble translating next to a wall in an otherwise quiescent liquid also experiences a lift force. This wall lift force, often simply referred to as wall force, has the general form:

$$F_{Wall} = \frac{2}{d_B} C_W \rho_L \alpha_G |\vec{u}_G - \vec{u}_L|^2, \tag{23}$$

where $\hat{y}$ is the unit normal perpendicular to the wall pointing into the fluid. The dimensionless wall force coefficient C_W depends on the distance to the wall y and is expected to be positive so the bubble is driven away from the wall. Based on the observation of single bubble trajectories in simple shear flow of glycerol water solutions Tomiyama et al. (1995) and later Hosokawa et al. (2002) concluded the functional dependence:

$$C_W(y) = f(Eo)\left(\frac{d_B}{2y}\right)^2, \tag{24}$$

where in the limit of small Morton number (Hosokawa et al. (2002))

$$f(Eo) = 0.0217Eo. \tag{25}$$

The experimental conditions on which Eq. 25 is based are $2.2 \leq Eo \leq 22$ and $-2.5 \leq log_{10}Mo \leq -6.0$ which is still different from the water-air system with $Mo = 2.63e-11$. A recent comparison of this and other distance-dependencies that have been proposed (Rzehak et al. (2012)) has nonetheless shown that good predictions could be obtained for a set of data on vertical upward pipe flow of air bubbles in water.

2.3.5. Virtual mass

The virtual mass is the inertia of the surrounding fluid that has to be taken into account when a bubble or particle is accelerated relative to the surrounding continuous phase:

$$F_{VM} = C_{VM}\alpha_G\rho_G(\frac{D\vec{u}_G}{Dt} - \frac{D\vec{u}_L}{Dt}), \tag{26}$$

where D/Dt denotes the substantial derivative. The coefficient C_{VM} is simply set to 0.5 as suggested by Mougin and Magnaudet (2002).

3. Setup

3.1. Experimental data

As experimental reference the results of bin Mohd Akbar et al. (2012) have been used. The experiments were executed in a rectangular water/air bubble column at ambient conditions. The ground plate is a rectangle of 240x72 mm and the water level is at 700 mm. The inlet is realized through needles at the bottom.

Measurements were performed for two superficial velocities, 3 mm/s and 13 mm/s, the integral void fraction for both conditions is below 10 %. The measurement plane is 500 mm above the inlet. The measured quantities are the liquid velocity, gas volume fraction and the turbulence intensity in the upward direction. Additionally, the bubble size distributions at the inlet and at the measurement plane were measured. The bubble size distributions are reproduced in Figure 1.

3.2. Simulation setup

3.2.1. Polydispersity and iMUSIG

The inhomogeneous multiple size group (iMUSIG) model as introduced by Krepper et al. (2008) assigns the bubble size classes used in the MUSIG model to different velocity groups. Each velocity group, therefore, has its own velocity field. This is important to describe effects like the bubble size dependent movement of the gas phase caused by the lift force.

As indicated in Figure 1 coalescence and break-up processes are not dominant for the present setup. Therefore, a simplified model can be used, consisting of two velocity groups each with its own set of mass- and momentum

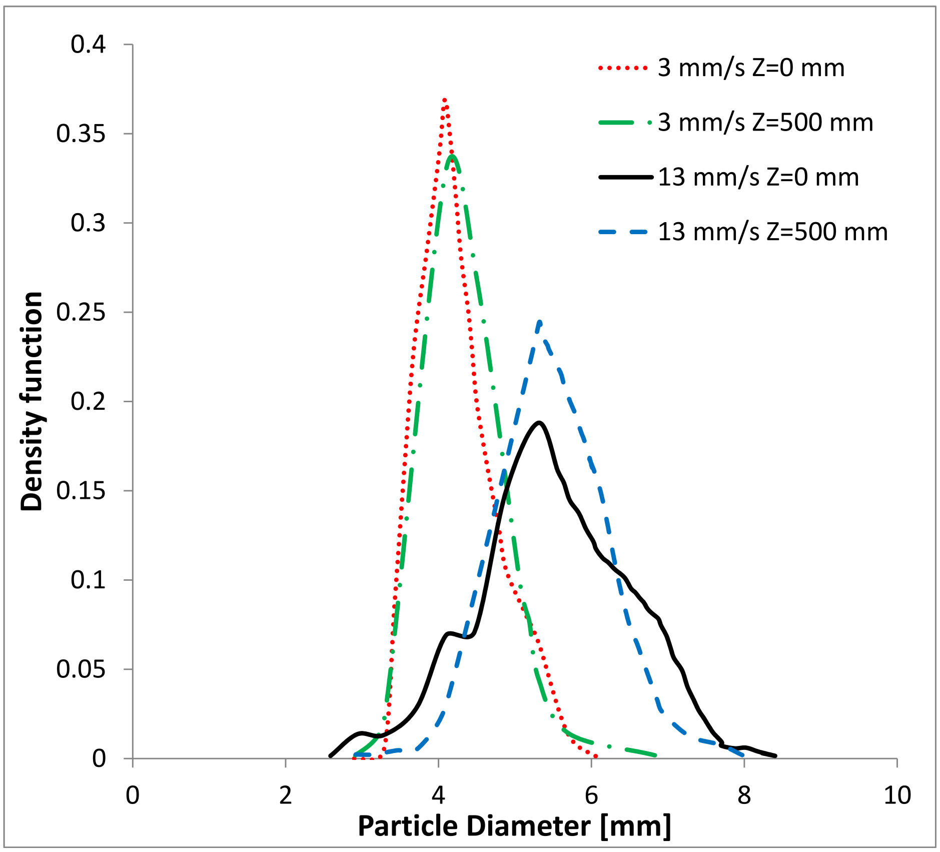

Figure 1: Density function of the bubble diameter in the experiment of bin Mohd Akbar et al. (2012) at different height levels

equations but with only as single bubble size class each. The groups are chosen in a way that the bubble size distributions are split up at the diameter where the lift force changes its sign. The resulting bubble classes for the case of 13 mm/s superficial velocity can be found in table 1.

	d_B	α	$Eo_\perp$	C_L
Bubble Class 1	5.3 mm	0.63	3	0.288
Bubble Class 2	6.3 mm	0.37	7.3	-0.116

Table 1: Used bubble classes

The case of 3 mm/s superficial velocity is treated as monodisperse, because almost all bubbles have a positive lift coefficient. The average bubble diameter for this case is 4.3 mm.

3.2.2. Solution method

The rectangular bubble column is discretized in structured rectangular volumes. The size of the volumes is determined after a mesh study which is shown below. The walls are treated as no slip condition for the continuous phase and slip condition for the dispersed phase. The top of the column is treated as a degassing boundary, which means a no penetration and slip condition for the continuous phase and an outlet for the dispersed phase. In this way the pressure remains variable over the top of the column, representing the different surface heights at different positions (Ansys (2013)).

The inlet is defined as surfaces at the bottom of the domain, representing the experimental needle setup. The surface that represents one needle is rectangular with an edge length of 4x4 mm. The gas volume flow is divided equally over all needles. The inlet velocity is naturally equal to gas volume flow divided by the total inlet surface.

For the spatial discretization a high resolution scheme is used (Ansys (2013)). For the transient discretization a second order backward Euler scheme is used.

3.3. Convergence criteria

To determine whether the results are independent of the total simulation time a convergence criterion is needed. Often a fixed total simulation time is taken as a convergence criterion. If this fixed simulation time is reached the simulation is defined as convergent. This simple method makes the assumption that a convergent state exists and that this state is reliably reached after the defined time. Therefore, this method is insufficient to investigate the convergence behavior of a simulation. Also this method is insufficient if it is unknown if the convergence is reliably reached after this time. Therefore, another convergence criterion is needed for the present investigations.

The convergence criterion is defined in a way that averages $\bar{f}$ taken over the simulation time T do not change significantly anymore when T is increased. The average over a finite time ζ is defined as

$$\bar{f}(\zeta) = \frac{1}{\zeta} \int_0^{\zeta} f(t) dt \ . \tag{27}$$

In particular, the averages $\bar{f}$ tend to a constant asymptote as ζ is increased. A reasonable convergence criterion can be defined by analyzing the distance between $\bar{f}(\zeta)$ and this constant asymptote.

Nevertheless, this constant asymptote which $\bar{f}(\zeta)$ is tending to with increasing ζ is not known. However, if $\bar{f}(\zeta)$ is tending to a constant asymptote, the values of $\bar{f}(\zeta)$ will change less with increasing ζ. For example, the difference between $\bar{f}(T-\Delta\zeta)$ and $\bar{f}(T)$ tends to zero with increasing simulation time T. If the difference between all values of $\bar{f}$ in the interval between $T-\Delta\zeta$ and T is evaluated, a trustworthy convergence criterion will be obtained. The effort of this procedure is reduced by comparing each value of $\bar{f}$ in this interval to an average of $\bar{f}$ over this interval. This is expressed mathematically by requiring that

$$\left|\frac{1}{\Delta\zeta}\int_{T-\Delta\zeta}^{T}\overline{f}(\zeta)d\zeta-\overline{f}(\zeta)\right|\leq\epsilon\ ;\ T-\Delta\zeta\leq\zeta\leq T\ . \tag{28}$$

As function f we choose the upward liquid velocity. Based on experience we choose $\Delta\zeta = 150s$ and ϵ to half of the experimental uncertainty (1.5 % of the experimental value) to obtain a good approximation without consuming excessive CPU-time. The convergence criterion is evaluated at two points, x_1 and x_2, which are chosen symmetric. Therefore, a criterion evaluating the symmetry of the obtained result can be defined:

$$\left|\overline{f}(x_1,\zeta)-\overline{f}(x_2,\zeta)\right|\leq 2\epsilon\ ,\ T-\Delta\zeta\leq\zeta\leq T\ . \tag{29}$$

This criterion is meaningful because the setup is symmetrical and a symmetric result is expected. It will be used in the further discussion.

4. Results

For transient simulations with subsequent averaging it must be guaranteed that the solution is independent of the simulation time, independent of the discretization and independent of the time step. The independence of the simulation time is guaranteed by using the convergence criterion presented in Section 3.3. In Section 4.1 and in Section 4.2 the mesh and time step study are presented. In Section 4.2 it is also shown that the time step study is strongly affected by using the virtual mass force. Accordingly, the role of the virtual mass force is investigated in Section 4.3. Finally, the influence of the multiphase turbulence modeling is investigated in Section 4.4 by comparing the above described modeling with source terms, the Sato model, and a model neglecting the bubble induced turbulence. Comparison with the experimental data is included in sections 4.3 and 4.4 in order to draw conclusions about the suitability of the modeling.

4.1. Mesh study

To obtain a mesh independent solution an intensive mesh study was performed using the model with source terms for the bubble induced turbulence and including the virtual mass force. An extract of this study for the case with a superficial velocity of 13 mm/s is shown in Figure 2. All simulations are converged using the defined convergence criterion. Four meshes are presented:

- an isotropic mesh with 4 mm edge length of each cell which contains around 200 000 cells,
- two anisotropic meshes, one with an edge length of 3 mm in depth and vertical direction and 4 mm in width direction with around 300 000 cells and the other with an edge length of 5 mm in depth and vertical direction and 4 mm in width direction with around 140 000 cells,
- a dilation in stream wise direction with 10 mm edge length in vertical

direction and 4 mm edge length in depth and width direction with 80 000 cells.

The mesh study is conducted by investigating the gas volume fraction, the upward liquid velocity and the turbulence intensity in the upward direction. Comparing the obtained values for the gas volume fraction and the upward liquid velocity even the coarse grid with 80 000 cells gives similar results as the finest mesh with 300 000 cells. The resolved turbulence intensity is a little bit different, but a clear trend with mesh size is not observable.

The upward turbulence intensity diagram consists of three curves which correspond to equation 12. The curve marked with 'resolved' corresponds to $\overline{\widetilde{w}'\widetilde{w}'}$, the curve marked with 'unresolved' to $\overline{\widetilde{w''w''}} = 2/3\overline{k_{mod}}$ and the curve marked with 'total' to $\overline{w'w'}$. The unresolved curve is the result that would be obtained if a stationary simulation would be performed. Further, the resolved curve represents the amount which is added through the transient simulation. The total curve represents the total turbulence intensity as it is obtained in the experiment.

The differences in the upward turbulence intensity occur close to the wall. Using the isotropic mesh and the finest mesh two peaks are noticeable at the walls. Using the two coarser meshes these wall peaks are less pronounced. With the coarsest mesh a slightly higher overall value is obtained. Nevertheless, deviations are quantitatively small.

Summarizing, the solution is mesh-independent already tor the isotropic mesh; hence, this is used for the further calculations. It should be noted that a mesh study is only possible if the solution is independent of the time step and vice versa. This circumstance was considered and the mesh study

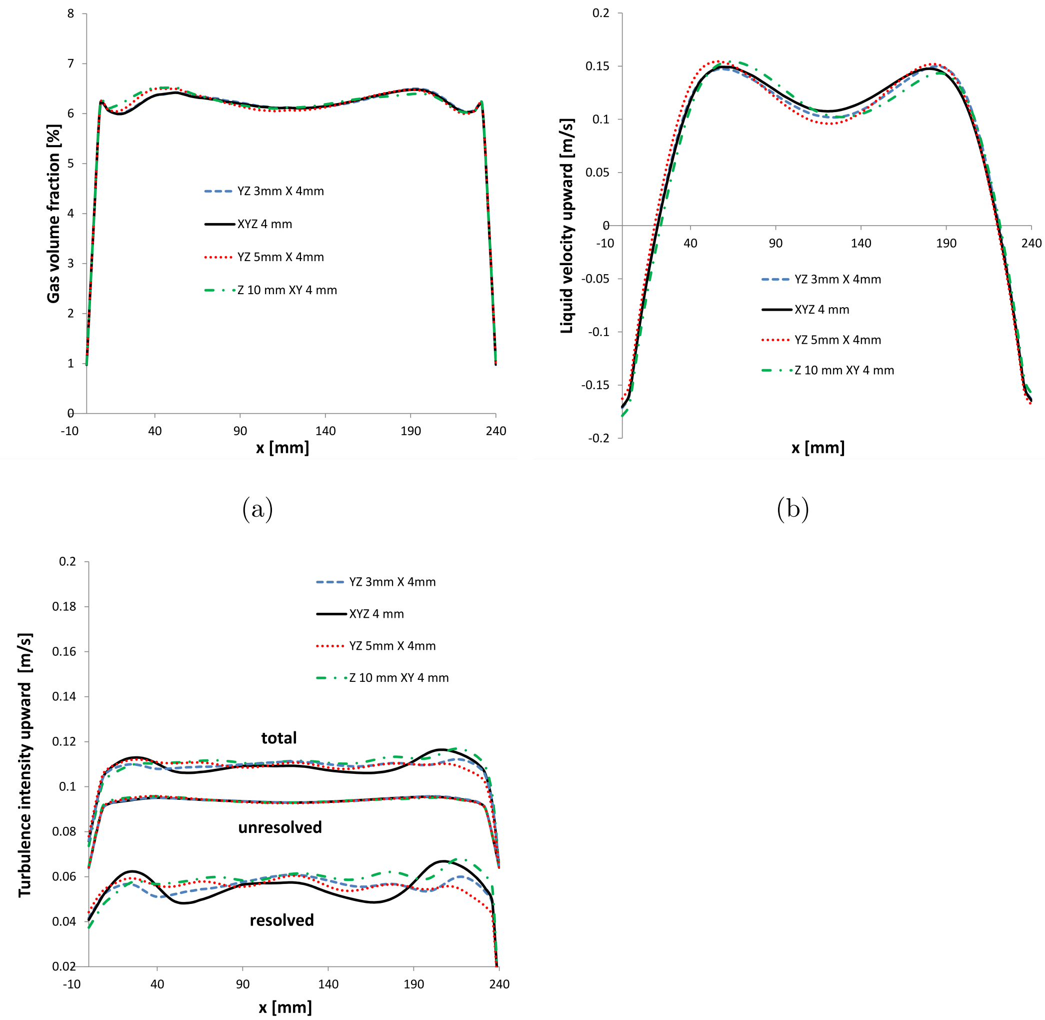

(a) (b)

(c)

Figure 2: Mesh study for 4 different meshes

was performed with sufficiently small time steps. Thus, the maximum root mean square of the Courant–Friedrichs–Lewy number over the domain was less than 2.2 for all meshes. As discussed in the next section this maximum value was found to be sufficient for independence on the time step.

4.2. Time step study

To find conditions under which the solution becomes independent of the time step a study is performed for 13 mm/s superficial velocity. Because it turns out that the time step is connected with the virtual mass force, both model variations including the virtual mass force and not including the virtual mass force are investigated. The difference between both model setups is discussed in detail in the next section.

To characterize the discretization of the problem in time and space the Courant–Friedrichs–Lewy number (CFL number, $CFL = |u|\frac{|\Delta x|}{\Delta t}$) is used. Because the velocity is a function of position and time so is the CFL number. To get a characteristic value, the root mean square (rms) of all CFL numbers in the computational domain is calculated. Further, the maximum and minimum $rms(CFL)$ numbers over time are given.

4.2.1. With virtual mass

The time study with the virtual mass force was performed in the range of $rms(CFL) = 0.8$ up to $rms(CFL) = 2.6$. The results are shown in Figure 3. For both simulations the convergence and symmetry criteria are reached.

Comparing the gas volume fraction and the liquid velocity profile for both time steps good accordance is reached. The volume fraction profile is nearly the same for both time steps. The liquid velocity profile differs a little bit

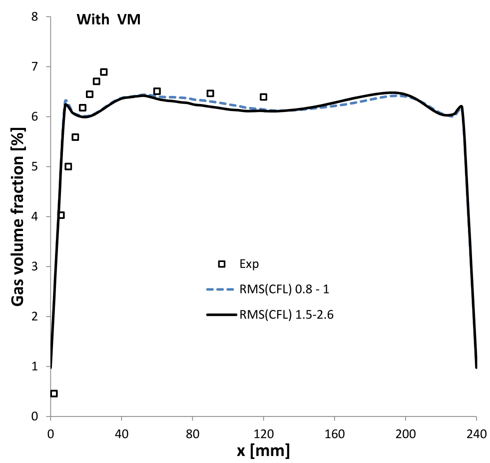

(a)

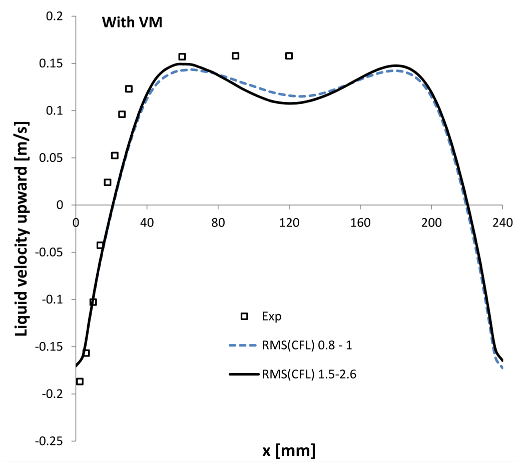

(b)

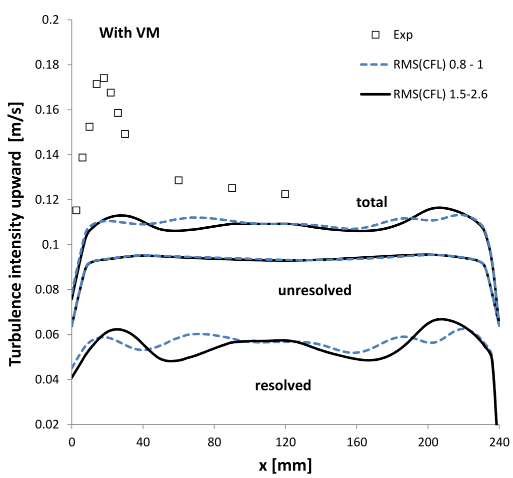

(c)

Figure 3: Time step study for different CFL numbers using the virtual mass force.

for the different time steps. The resolved upward turbulence profiles for the different time steps are slightly different, the peak near the wall being slightly higher for the larger value of $rms(CFL)$. The unresolved turbulence profiles are equal for both time steps. Since the unresolved contribution constitutes a major part of the total turbulence intensity, the curves for this quantity are in good agreement as well.

In conclusion, when the virtual mass force is included, the solution becomes independent of the time step for $rms(CFL) \lesssim 2.6$.

4.2.2. Without virtual mass

The time step study without using the virtual mass force was performed in the range of $rms(CFL) = 0.6$ up to $rms(CFL) = 8$. In Figure 4 selected results of the time step study are shown. All simulations are convergent using the convergence criterion defined in Section 3.3.

Comparing the curves for the gas volume fraction, the upward liquid velocity and the upward turbulence intensity obtained using different time steps significant differences can be seen. In particular, the simulations using $rms(CFL)$ above 1 do not fulfill the expected symmetry according to the criterion given in Section 3.3. In contrast, the simulation using $rms(CFL)$ below 1 do fulfill this criterion. Also, in contrast to the simulations using $rms(CFL)$ above 1 the simulation using $rms(CFL)$ below 1 gives two peaks in all three quantities. Comparing the simulation using $rms(CFL)$ below 1 with the simulations including the virtual mass force in Figure 3, very small differences are seen.

In conclusion, when the virtual mass force is neglected, a solution that is independent of the time step is achieved provided that the condition

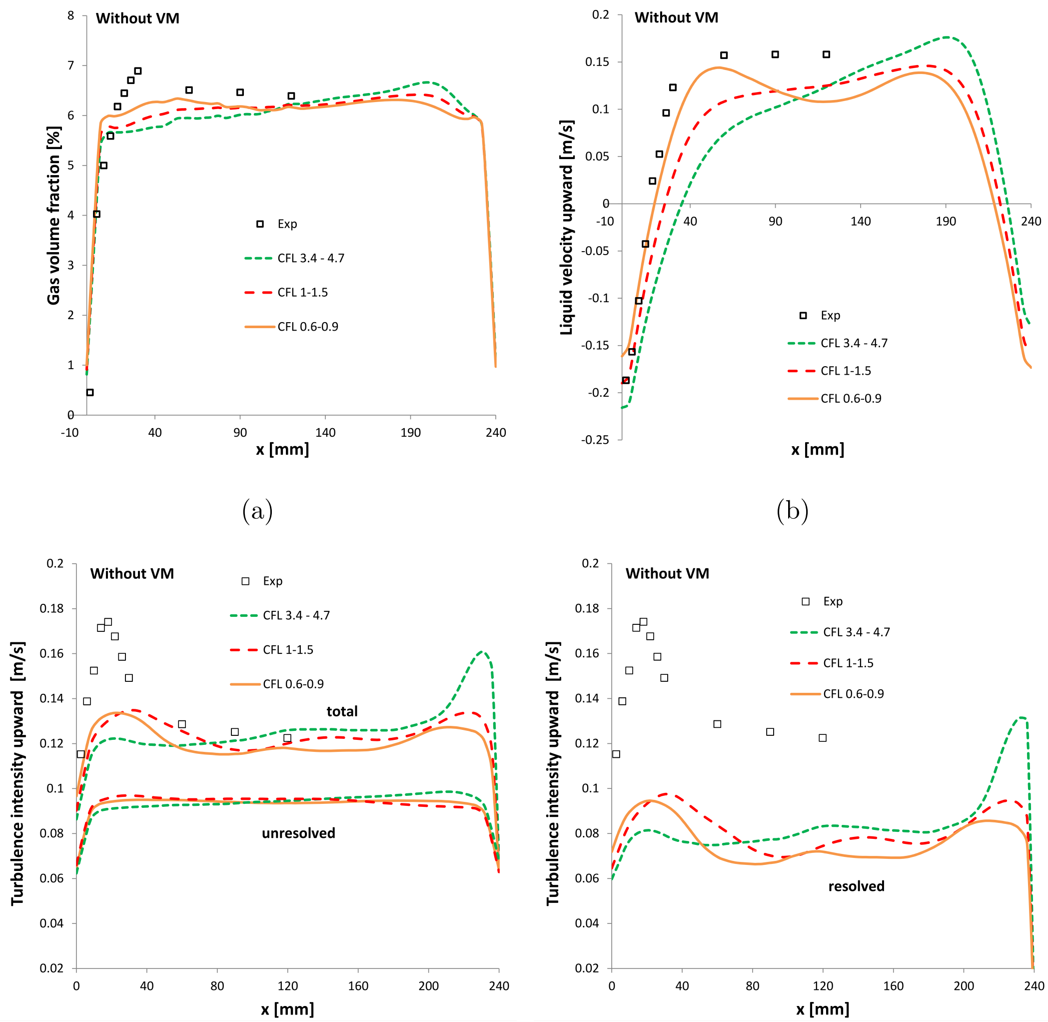

(a) (b)

(c) (d)

Figure 4: Time study for different $rms(CFL)$-numbers without using the virtual mass force.

$rms(CFL) < 1$ is satisfied.

4.3. Effect of the virtual mass force

In the previous section it was pointed out that the transient simulations with the URANS approach with and without virtual mass force are time step independent under certain requirements. In this section the simulations with and without using the virtual mass force are compared and the effect of the virtual mass force is discussed.

In Figure 5 the results of the simulations with and without virtual mass force are shown for both superficial velocities 13 mm/s and 3 mm/s. For 3 mm/s superficial velocity the results obtained with and without virtual mass force are the same. This is different for 13 mm/s superficial velocity. Therefore, the following discussion is only related to the 13 mm/s case.

Looking at the liquid velocity profiles for the case with 13 m/s superficial velocity, no differences between the model variants with and without virtual mass force are seen. Distinct peaks in each side can be observed in the profiles. At the same positions as in the liquid velocity profile, broad maxima can be observed in the gas volume fraction profile for both model variants. In addition, if the model variant including the virtual mass force is used, the gas volume fraction profile will exhibit sharp peaks almost at the wall. In contrast, if the model variant neglecting the virtual mass force is used, these sharp peaks will nearly vanish.

The broad maxima near the center in the gas volume fraction profile can be explained by the stability criterion of Lucas et al. (2005), which is derived analytically from the force balance, depending on the volume fraction of big and small bubbles. This stability criterion is based on the change of sign

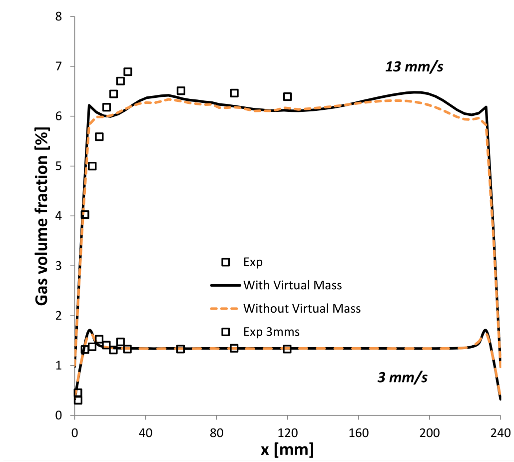

(a)

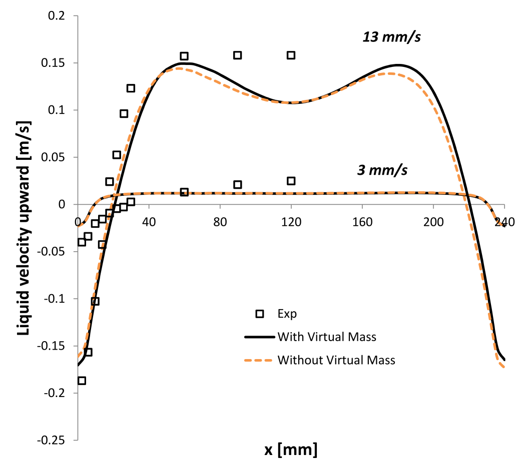

(b)

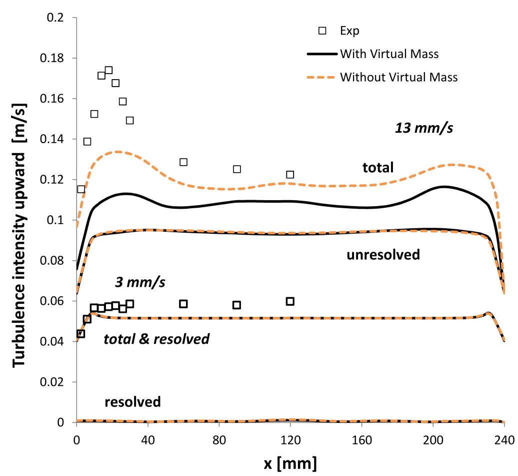

(c)

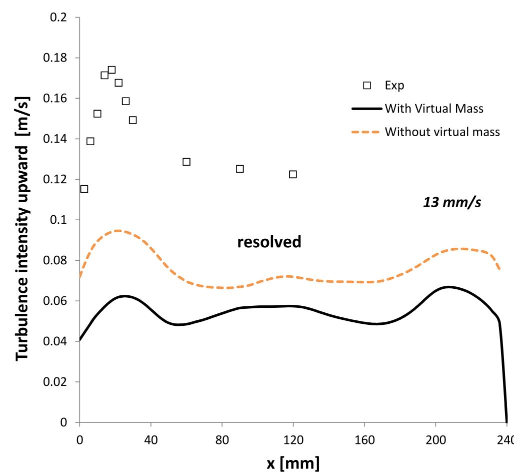

(d)

Figure 5: Comparison between using the virtual mass force and not using the virtual mass force for a superficial velocity of 13 mm/s and 3 mm/s. The curves for using the virtual mass force and not using the virtual mass force for the 3 mm/s case are of the top of each other.

in the lift force coefficient and is therefore connected to the gradient of the liquid velocity. By solving separate momentum equations for big and small bubbles, as was pointed out in Section 3.2.1, this effect is also taken into account in the present simulations. Because the liquid velocity gradient and the volume fractions of big and small bubbles depend on the local position, the stability criterion of Lucas et al. (2005) has to be evaluated locally.

In the lower section of the column, the big and small bubbles are not separated. Due to the the wall shear stress and the resulting liquid velocity gradient the big and small bubbles separate with increasing height. The big bubbles move to the center, the small bubbles move to the wall. Consequently, the local concentration of the big bubbles rises from the wall towards the center of the column. Further, away from the wall the movement of the big bubbles is slowed down, because of the decreasing liquid velocity gradient. As a result, the big bubbles accumulate and the local void fraction of the big bubbles increases at the same point. Due to buoyancy this is accompanied by an increase of the local liquid velocity. If the stability criterion described in Lucas et al. (2005) is exceeded, a distinct liquid velocity peak will be formed at this point. Once this has happened the large bubbles cannot move further towards the center because of the negative lift coefficient. This means that steady profiles with peaks in the liquid velocity and gas fraction are established.

The separation of big and small bubbles can also explain the gas volume fraction profile, as can be seen from Figure 5. In the gas volume fraction profile the near wall peak is caused by the accumulation of the small bubbles and the broad maximum halfway between the wall and the center is caused by the accumulation of the big bubbles.

Figure 5 also shows the upward turbulence intensity. For the case with 13 mm/s superficial velocity also peaks near the wall can be observed. These peaks are not at the same position as the peaks in the liquid velocity profile and might be less affected by the separation of big and small bubbles. The near wall peaks in the upward turbulence profile are nearly at the point where the liquid velocity passes through the zero line which is the point of the highest liquid velocity gradient. Also the resolved upward turbulence profile is higher in general for the simulation without using the virtual mass force. Therefore, by using the virtual mass force a damping of the liquid velocity fluctuations is introduced.

All in all, including or neglecting the virtual mass force leads to different results for the case with 13 mm/s superficial velocity. The gas volume fraction profile is quantitatively almost the same for both model variants. However, not using the virtual mass force the near wall peak in the gas volume fraction profile nearly vanishes. The resolved upward turbulence intensity profiles have the same shape, but quantitatively the resolved upward turbulence intensity is higher if the virtual mass force is neglected. While the gas volume fraction and the upward turbulence profiles are different, the liquid velocity profile is nearly the same for both model variants. In contrast to the case with 13 mm/s superficial velocity, all profiles obtained for the 3 mm/s superficial velocity are the same. The equality might be explained by the fact that the resolved upward turbulence intensity at the measurement plane is nearly zero for 3 mm/s superficial velocity. Consequently, nearly no fluctuation is resolved and the acceleration is nearly zero. As a result, the virtual mass force is nearly zero.

4.4. Bubble induced turbulence modeling

The influence of the bubble induced turbulence (BIT) model on the URANS simulations is shown in this section. The bubble induced turbulence modeling with source terms by Rzehak and Krepper (2013b), as described in Section 2.1.1, the addition of a turbulent viscosity by Sato et al. (1981), as described in Section 2.1.2 and a model neglecting the bubble induced turbulence are compared. At first the results for the case with 13 mm/s superficial velocity are discussed, afterwards the results for the case with 3 mm/s superficial velocity. All simulations are performed with the virtual mass force and fulfill the above defined convergence and symmetric criteria.

The results for 13 mm/s superficial velocity are shown in Figure 6. For a better readability the resolved part of the upward turbulent kinetic energy is shown in a separate diagram. The gas hold up is quantitatively very similar for all considered models, but the sharp near wall peak is pronounced only for turbulence modeling with source terms. The liquid velocity using the Sato model and using no BIT model is lower than the experiments and the profile obtained with the BIT model by Rzehak and Krepper (2013b). Qualitatively the different model approaches show the same behavior. However, using the Sato model and using no BIT model both peaks in the liquid velocity profile are shifted towards the center and are smaller.

Remarkably the quantity of the resolved turbulence intensity is very similar for all used BIT models. Concerning the shape of the profiles, the peaks are shifted to the center and are smaller for the models not using the source terms. The total upward turbulence intensity is underpredicted by all models but significantly closer to the data for the models with source terms. Differences between the Sato model and neglecting BIT are small in comparison.

The differences between the different approaches to BIT modeling observed in Figure 6 can be explained by considering the turbulent viscosity which is shown in Figure 7. As the resolved turbulence intensity is comparable for all models, only the unresolved part of the turbulent viscosity is shown. It can be seen from Figure 7 that for the BIT modeling using source terms the turbulent viscosity is the lowest. This is caused by a higher turbulent dissipation rate (not shown). Looking only at the turbulent kinetic energy which is the highest for the modeling using source terms, the opposite effect on the turbulence viscosity may have been expected. The reason for the behavior observed in the simulations must be sought in the ϵ respectively in the ω source term. Further, as expected, the turbulent viscosity using a BIT model with additional viscosity is the highest. Using no BIT model the level of the turbulent viscosity is between the other approaches.

The higher turbulent viscosity obtained with the Sato model and using no BIT model is causing a reduced amplitude in the lower liquid velocity profile compared to the BIT modeling with source terms, as shown in Figure 6. In particular, using the Sato model and using no BIT model the liquid velocity gradient near the wall is smaller compared to the experiment and the BIT modeling with source terms. Consequently, the instability caused by the separation by the big and small bubbles, as discussed in Section 4.3, is also shifted to the center. Therefore, the observed velocity peaks using the Sato model and using no BIT model observed in Figure 6 are shifted to the

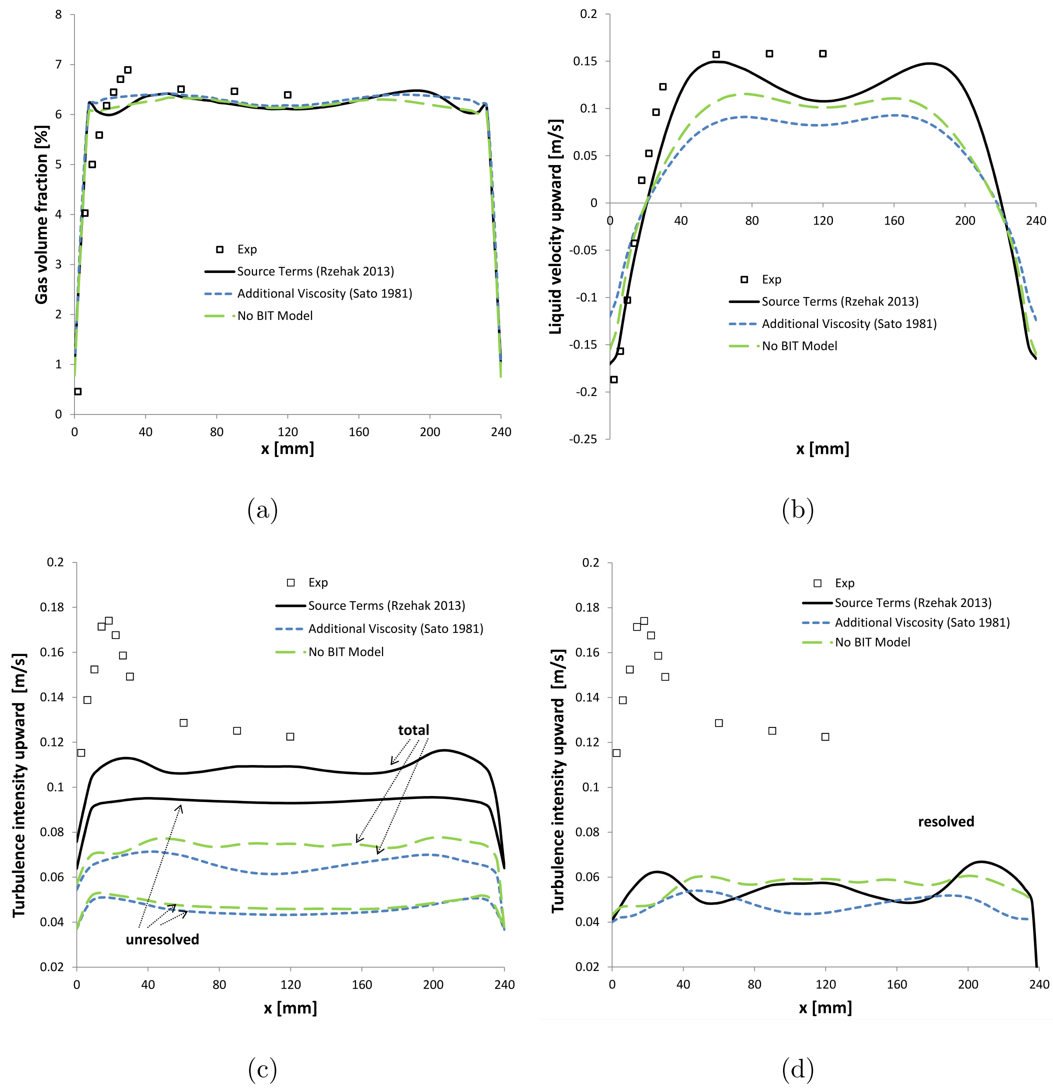

Figure 6: Comparison of different bubble induced turbulence modeling approaches for 13 mm/s superficial velocity.

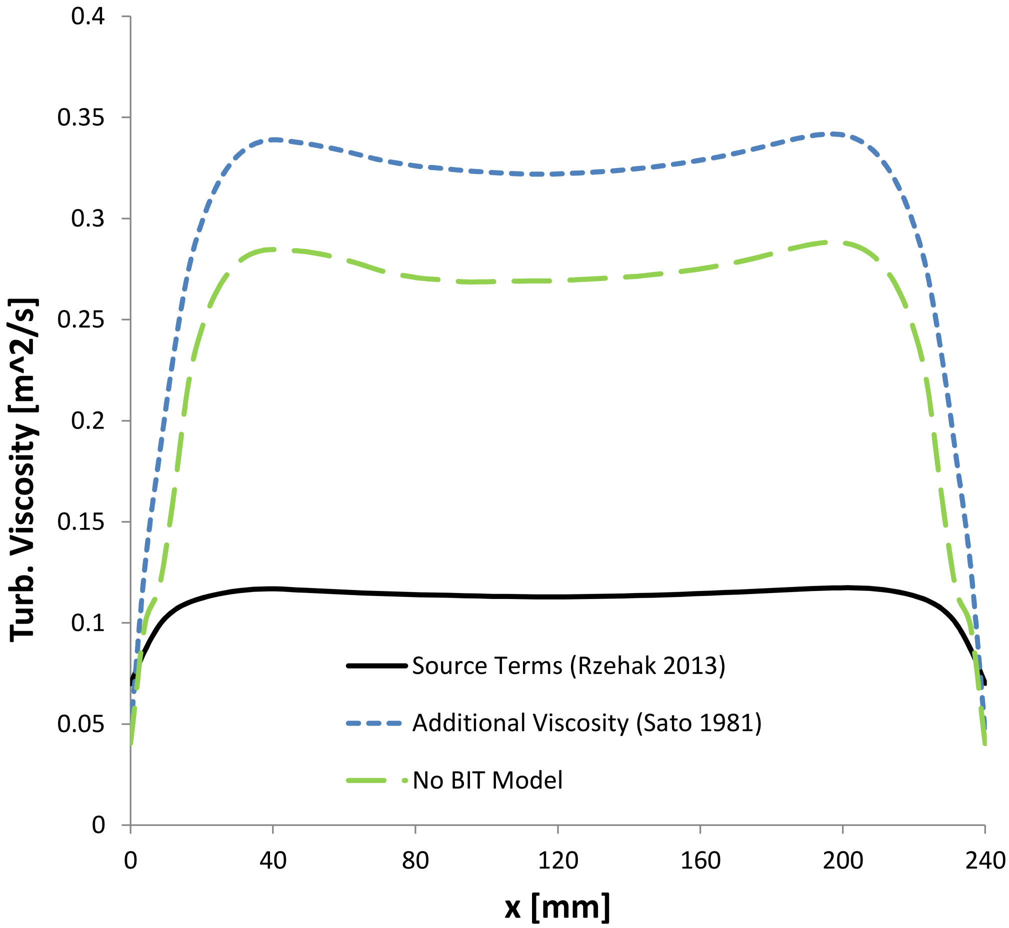

Figure 7: Unresolved turbulent viscosity for different modeling approaches for 13 mm/s superficial velocity.

center.

Another effect of the higher turbulent viscosity that is obtained with the Sato model and using no BIT model (see Figure 7) is a higher turbulent dispersion of the bubbles. As described in Section 2.3.3, the turbulent dispersion force is proportional to the turbulent viscosity and to the gradient of the gas volume fraction. It acts towards a more uniform distribution of gas. As a result, the peaks in the gas volume fraction profiles shown in Figure 6 are flatter when using the Sato model or using no BIT model compared to the BIT modeling with source terms. Consequently, the liquid velocity peak is also flatten when using the Sato model or using no BIT model. In particular, the near wall peak of the small bubbles that can be observed for the BIT modeling with source terms in Figure 6 nearly vanishes when using the Sato model or using no BIT model.

For the case with 3 mm/s superficial velocity the liquid velocity and the gas volume fraction profiles obtained by using the different BIT model approaches are nearly the same. Therefore, only the total upward turbulence intensity is discussed in the following. The results are shown in Figure 8.

It can be seen from the Figure 8 that the upward turbulence intensity is quite well predicted by the BIT modeling with source terms. In contrast, using the Sato model or using no BIT model the turbulence intensity for the case with 3 mm/s superficial velocity is considerably underpredicted. This is the same trend as can be observed for the case with 13 mm/s superficial velocity.

Summarizing, the best prediction of the turbulence intensity is obtained by the turbulence modeling with source terms, using the formulation of Rze-

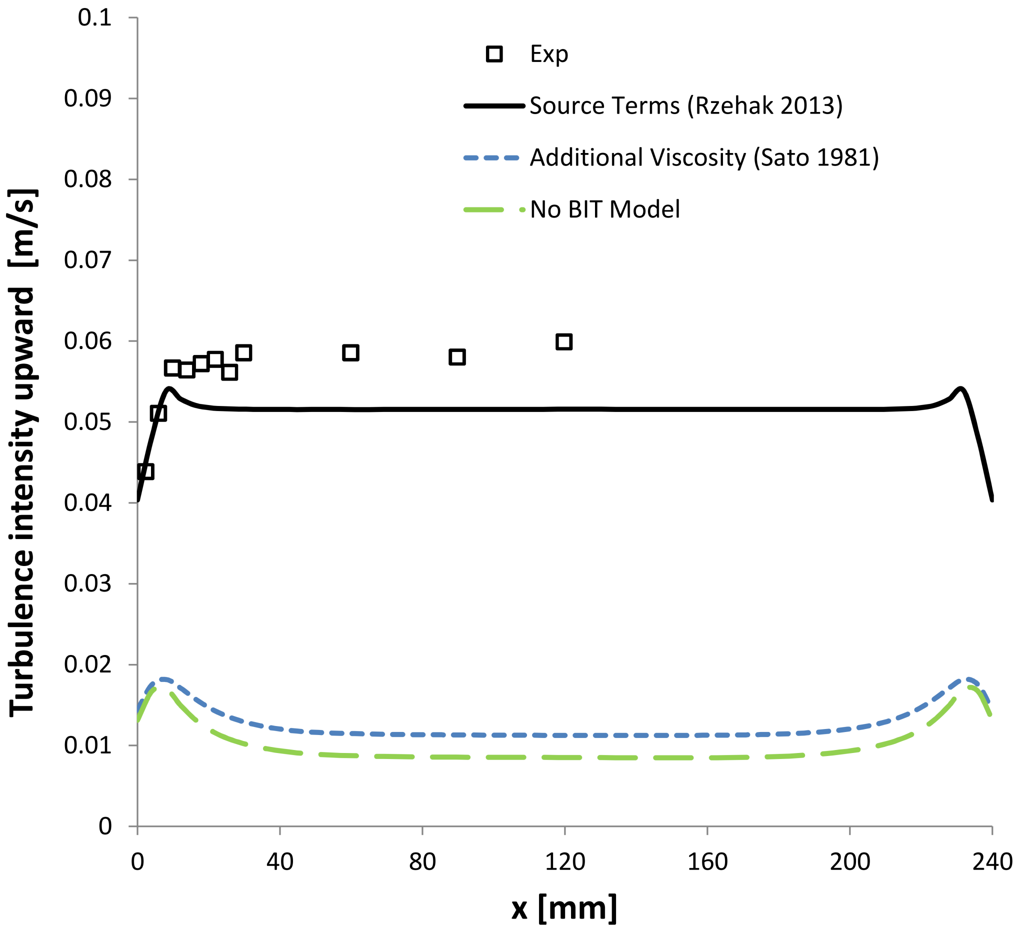

Figure 8: Comparison of the total upward turbulence intensity for different bubble induced turbulence modeling approaches for 3 mm/s superficial velocity.

hak and Krepper (2013b). The position of the peak in the upward turbulence intensity profile for 13 mm/s superficial velocity is well reproduced. Using the Sato model or no BIT model the upward turbulence intensity is considerably underpredicted compared to the experimental data. Furthermore, there is no peak in the upward turbulence intensity for 13 mm/s superficial velocity.

The turbulent viscosity obtained for this case with the Sato model or using no BIT model is significantly higher than the obtained turbulent viscosity using the BIT modeling with source terms using the formulation of Rzehak and Krepper (2013b). Consequently, the liquid velocity profiles are less steep using the Sato model and using no BIT model compared to the BIT modeling with source terms. Compared to the experimental data the liquid velocity is underpredicted using the Sato model or no BIT model, but predicted well by the modeling using source terms.

5. Discussion and conclusion

Transient simulations with RANS-based turbulence modeling (URANS) were performed to model large scale flow structures in bubble columns. The model approach was intensively discussed by distinguishing resolved and unresolved turbulent kinetic energy. The simulations were performed in a monodisperse and a polydisperse bubbly flow regime and compared with experimental data. The independence of the solution concerning simulation time, time step length and mesh size was in detail discussed by introducing a convergence criterion and a symmetry criterion. A set of closure models recommended by Rzehak et al. (2013) intended to provide a general and predictive modeling for bubbly flow was used.

In the poyldisperse regime with higher superficial velocity the resolved structures obtained by using the URANS approach give important contributions to the turbulence. Including these contributions by the transient simulations gives better results compared to the experimental data. The improvement by taking the resolved structures into account is found for all used approaches to bubble induced turbulence modeling. In a previous study (Ziegenhein et al. (2013a)) based on a steady state approach neglecting the resolved contributions, all commonly used bubble induced turbulence models under predict the turbulence intensity for this experimental setup. In the monodisperse bubbly flow regime with lower superficial gas velocity the very good match between simulation and experimental results that has be reached by a steady state simulation (Ziegenhein et al. (2013a)) is also achieved by using the URANS approach, because for this case the contribution of the resolved scales is only small.

In particular, the virtual mass force and the bubble induced turbulence modeling, and their influence on the resolved structures were investigated. Different behavior was observed depending on whether the virtual mass force is included or neglected in the model. Consequently, it was pointed out that the virtual mass force is not negligible in general and, therefore, the virtual mass force has to be added to the closure model set published by Rzehak et al. (2013).

Comparing different bubble induced turbulence modeling approaches, the approach using source terms in the turbulence equations using the model recommended by Rzehak et al. (2013) gives better results compared to the experimental data than the other modeling approaches. The influence of the bubble induced turbulence on the resolved turbulence intensity is rather small. This is mainly due to a different value of the turbulent viscosity.

5.1. Acknowledgment

This work was funded by the Helmholtz Association within the frame of the Helmholtz Energy Alliance "Energy Efficient Chemical Multiphase Processes".

Nomenclature

C_D	drag coefficient
$C_{\epsilon B}$	model constant
CFL	Courant-Friedrichs-Lewy number
C_L	lift coefficient
C_μ	shear induced turbulence coefficient
C_{VM}	virtual mass coefficient
C_W	wall force coefficient
d	diameter $[m]$
Eo	Eötvös number
F_{Disp}	turbulent dispersion force $[N\ m^{-3}]$

F_{Drag}	drag force $[N\ m^{-3}]$
F_{Lift}	lift force $[N\ m^{-3}]$
F_{VM}	virtual mass force $[N\ m^{-3}]$
F_{Wall}	wall force $[N\ m^{-3}]$
g	gravity $[m\ s^{-2}]$
k	turbulence kinetic energy $[m^2\ s^{-2}]$
Mo	Morton number
Re	Reynolds number
S^{ϵ}	ϵ-source term $[kg\ m^{-1}\ s^{-4}]$
S^{k}	k-source term $[kg\ m^{-1}\ s^{-3}]$
S^{ω}	ω-source term $[kg\ m^{-3}\ s^{-2}]$
T	simulation time $[s]$
t	time $[s]$
u	velocity $[m\ s^{-1}]$
w	velocity component $[m\ s^{-1}]$
$\vec{x}$	position vector $[m]$
x	horizontal position $[mm]$
y	wall distance $[m]$

Greek letters

α — gas void fraction

ϵ — real number > 0

ϵ — turbulence dissipation rate $[m^2\ s^{-3}]$

μ — dynamic viscosity $[kg\ m^{-1}\ s^{-1}]$

ω — specific turbulence dissipation rate $[s^{-1}]$

ρ — density $[kg\ m^{-3}]$

σ — surface tension $[N\ m^{-1}]$

σ_{TD} — turbulent dispersion coefficient

τ — time scale $[s]$

Subscripts

B — bubble

G — gas

k — k-th element of a set

L — liquid

$\perp$ — perpendicular to main motion

Appendix A. Governing conservation and turbulence equations

We assume that there is no mass transfer between the phases and the flow is isothermal without heat transfer. Therefore, only the conservation of mass, momentum and the turbulence equations have to be considered. The turbulence equations refer only to the liquid phase.

Appendix A.1. Conservation of momentum

The momentum balance of phase j is given by

$$\begin{aligned}&\frac{\partial}{\partial t}\left(\alpha_j \rho_j \vec{u}_j\right) + \nabla \cdot \left(\alpha_j \rho_j \vec{u}_j \vec{u}_j\right)\\&= -\alpha_j \nabla p + \nabla \cdot \tau_j + \alpha_j \rho_j \vec{g} + F_j^{Drag} + F_j^{Lift} + F_j^{VM} + F_j^{Wall} + F_j^{TD}, \quad \text{(A.1)}\end{aligned}$$

where τ_j is the stress tensor of the j-th phase.
Conservation of momentum requires that

$$\sum_k F_j^{Drag} + F_j^{Lift} + F_j^{VM} + F_j^{Wall} + F_j^{TD} = 0. \quad \text{(A.2)}$$

The mass balance of phase j is simply

$$\frac{\partial}{\partial t}\left(\alpha_j \rho_j\right) + \nabla\left(\alpha_j \rho_j u_j\right) = 0. \quad \text{(A.3)}$$

Appendix A.2. Turbulence equations

We here use the SST $k-\omega$ model which is obtained by a blending of $k-\epsilon$ and $k-\omega$ models. According to Menter et al. (2003) the transport equations for k and ω are

$$\frac{\partial}{\partial t}\left(\rho k\right) + \nabla\left(\rho k u\right) = S_k + \tilde{P}_k - Y_k + \nabla\left(\left(\mu + \sigma_k \mu_t\right) \nabla k\right) \quad \text{(A.4)}$$

$$\frac{\partial}{\partial t}(\rho\omega) + \nabla(\rho\omega u) = S_\omega + P_\omega - Y_\omega + \nabla((\mu + \sigma_\omega \mu_t)\nabla k) + D_\omega. \qquad \text{(A.5)}$$

The terms $\tilde{P}_k$ and P_ω represent the generation of k respective ω. The terms Y_k and Y_ω represent the dissipation of k and ω, respectively. The cross diffusion term D_ω arises due to the blending. Since all of these terms are the same as for the single phase problem, detailed information can be found in Menter et al. (2003). The terms S_k and S_ω are source terms which represent the bubble induced turbulence modeling.

Ansys, 2013. CFX 14.5 manual: CFX-Solver modeling guide. Ansys, Inc.

Bothe, D., Schmidtke, M., Warnecke, H.J., 2006. Vof-simulation of the lift force for single bubbles in a simple shear flow. Chem. Eng. Technol. 29, 1048.

Burns, A., Frank, T., Hamill, I., Shi, J.M., 2004. The favre averaged drag model for turbulent dispersion in eulerian multi-phase flows, in: 5th International Conference on Multiphase Flow, ICMF04, Yokohama, Japan, May 30-June 4, 2004, Paper No. 392.

Ekambara, K., Dhotre, M.T., Joshi, J.B., 2005. Cfd simulations of bubble column reactors: 1d, 2d and 3d approach. Chemical Engineering Science 60, 6733–6746. doi:10.1016/j.ces.2005.05.047.

Hosokawa, S., Tomiyama, A., Misaki, S., Hamada, T., 2002. Lateral migration of single bubbles due to the presence of wall, in: Proc. ASME Joint U.S.-European Fluids Engineering Division Conference (FEDSM2002), Montreal, Quebec, Canada, p. 855.

Ishii, M., Zuber, N., 1979. Drag coefficient and relative velocity in bubbly, droplet or particulate flows. AlChE Journal 25, 843.

Jakobsen, H.A., Lindborg, H., Dorao, C.A., 2005. Modeling of bubble column reactors: Progress and limitations. Ind. Eng. Chem. Res. 44, 5107.

Joshi, J.B., Deshpande, N.S., Dinakar, M., Phanikumar, D.V., 2001. Hydrodynamic stability of multiphase reactors, in: Advances in Chemical Engineering. Academic. volume 26, p. 1.

Joshi, J.B., Vitankar, V.S., Kulkarni, A.A., Dhotre, M.T., Ekambara, K., 2002. Coherent flow structures in bubble column reactors. Chemical Engineering Science 57, 3157.

Julia, J.E., Hernandez, L., Chiva, S., Vela, A., 2007. Hydrodynamic characterization of a needle sparger rectangular bubble column: Homogeneous flow, static bubble plume and oscillating bubble plume. Chemical Engineering Science 62, 6361–6377. doi:10.1016/j.ces.2007.07.055.

Krepper, E., Beyer, M., Frank, T., Lucas, D., Prasser, H.M., 2009. Cfd modelling of polydispersed bubbly two-phase flow around an obstacle. Nuclear Engineering and Design 239, 2372–2381.

Krepper, E., Lucas, D., Frank, T., Prasser, H.M., Zwart, P., 2008. The inhomogeneous musig model for the simulation of polydispersed flows. Nuclear Engineering and Design 238, 1690–1702.

Launder, B., Spalding, D., 1974. The numerical computation of turbulent flows. Computer Methods in Applied Mechanics and Engineering 3, 269–289. doi:http://dx.doi.org/10.1016/0045-7825(74)90029-2.

Liao, Y., Lucas, D., 2010. A literature review on mechanisms and models for the coalescence process of fluid particles. Chemical Engineering Science 65, 2851.

Liao, Y., Lucas, D., Krepper, E., Schmidtke, M., 2011. Development of a generalized coalescence and breakup closure for the inhomogeneous musig model. Nuclear Engineering and Design 241, 1024–1033.

Lucas, D., Prasser, H.M., Manera, A., 2005. Influence of the lift force on the stability of a bubble column. Chemical Engineering Science 60, 3609 – 3619.

Lucas, D., Tomiyama, A., 2011. On the role of the lateral lift force in poly-dispersed bubbly flows. International Journal of Multiphase Flow 37, 1178.

Masood, R., Delgado, A., 2014. Numerical investigation of the interphase forces and turbulence closure in 3d square bubble columns. Chemical Engineering Science , –doi:http://dx.doi.org/10.1016/j.ces.2014.01.004.

Menter, F., Kuntz, M., Langtry, R., 2003. Ten years of industrial experience with the sst turbulence model. Turbulence, heat and mass transfer 4, 625–632.

bin Mohd Akbar, M.H., Hayashi, K., Hosokawa, S., Tomiyama, A., 2012. Bubble tracking simulation of bubble-induced pseudoturbulence. Multiphase Science and Technology 24, 197–222.

Mougin, G., Magnaudet, J., 2002. The generalized kirchhoff equations and their application to the interaction between a rigid body and an arbitrary time-dependent viscous flow. International Journal of Multiphase Flow 28, 1837.

Mudde, R.F., 2005. Gravity-driven bubbly flows. Annual Review of Fluid Mechanics 37, 393–423.

Rzehak, R., Krepper, E., 2013a. Cfd modeling of bubble-induced turbulence. International Journal of Multiphase Flow 55, 138–155.

Rzehak, R., Krepper, E., 2013b. Closure models for turbulent bubbly flows: A cfd study. Nuclear Engineering and Design 265, 701–711.

Rzehak, R., Krepper, E., Lifante, C., 2012. Comparative study of wall-force models for the simulation of bubbly flows. Nuclear Engineering and Design 253, 41–49.

Rzehak, R., Liao, Y., Lucas, D., Krepper, E., 2013. Baseline model for cfd of dispersed bubbly flow, in: 15th International Topical Meeting on Nuclear Reactor Thermal-hydraulics, NURETH-15, Pisa, Italy, pp. NURETH15–315.

Sato, Y., Sadatomi, M., Sekoguchi, K., 1981. Momentum and heat transfer in two-phase bubble flow i: Theory. Int. J. Multiphase Flow 7, 167.

Sokolichin, A., Eigenberger, G., 1999. Applicability of the standard k-epsilon turbulence model to the dynamic simulation of bubble columns: Part i. detailed numerical simulations. Chemical Engineering Science 54, 2273.

Spalart, P., 2000. Strategies for turbulence modelling and simulations. International Journal of Heat and Fluid Flow 21, 252–263. doi:doi:10.1016/S0142-727X(00)00007-2.

Tabib, M.V., Roy, A., Joshi, J., 2008. Cfd simulation of bubble column-an analysis of interphase forces and turbulence models. Chemical Engineering Journal 139, 589–614.

Tomiyama, A., 2002. Single bubbles in stagnant liquids and in linear shear flows, in: Workshop on Measurement Techniques for Steady and Transient Multiphase Flows, Forschungszentrum Rossendorf.

Tomiyama, A., Kataoka, I., Zun, I., Sakaguchi, T., 1998. Drag coefficients of single bubbles under normal and micro gravity conditions. JSME International Journal B 41, 472.

Tomiyama, A., Sou, A., Zun, I., Kanami, N., Sakaguchi, T., 1995. Effects of etvs number and dimensionless liquid volumetric flux on lateral motion of a bubble in a laminar duct flow, in: Serizawa, A., Fukano, T., Bataille, J. (Eds.), Advances in multiphase flow, Elsevier. p. 3.

Wellek, R.M., Agrawal, A.K., Skelland, A.H.P., 1966. Shape of liquid drops moving in liquid media. AlChE Journal 12, 854.

Yeoh, G.H., Tu, J., 2010. Computational techniques for multiphase flows. Elsevier.

Ziegenhein, T., Lucas, D., Rzehak, R., Krepper, E., 2013a. Closure relations for cfd simulation of bubble columns, in: 8th International Conference on Multiphase Flow ICMF2013, Jeju, Korea.

Ziegenhein, T., Rzehak, R., Krepper, E., Lucas, D., 2013b. Numerical simulation of polydispersed flow in bubble columns with the inhomogeneous multi-size-group model. Chemie Ingenieur Technik 85, 1080–1091. doi:10.1002/cite.201200223.

Zun, I., 1980. The transverse migration of bubbles influenced by walls in vertical bubbly flow. International Journal of Multiphase Flow 6, 583.